# Composite beam finite element based on the proper generalized decomposition

P. Vidal, L. Gallimard, O. Polit

# Composite beam finite element based on the Proper Generalized Decomposition

P. Vidal *, L. Gallimard, O. Polit

*Laboratoire Energétique, Mécanique, Electromagnétisme, Université Paris Ouest Nanterre-La Défense, 50 rue de Sèvres, 92410 Ville d'Avray, France*

A B S T R A C T

In this paper, a finite element based on the Proper Generalized Decomposition is presented for the analysis of bi-dimensional laminated beams. We propose to approximate the displacement field as a sum of separated functions of $x$ (axial coordinate) and $z$ (transverse coordinate). This choice yields to an iterative process that consists of computing a product of one-dimensional functions at each iteration. Mechanical tests for thin/thick laminated and sandwich beams are presented in order to evaluate the capability of this method. Both convergence rate and accuracy are discussed. The influence of the numerical layers is also assessed.

## 1. Introduction

Composite and sandwich structures are widely used in the industrial field due to their excellent mechanical properties, especially their high specific stiffness and strength. In this context, they can be subjected to severe mechanical loads. For composite design, accurate knowledge of displacements and stresses is required. So, it is important to take into account effects of the transverse shear deformation due to the low ratio of transverse shear modulus to axial modulus, or failure due to delamination. In fact, they can play an important role on the behavior of structures in services, which leads to evaluate precisely their influence on local stress fields in each layer, particularly on the interface between layers.

According to published research, various theories in mechanics for composite or sandwich structures have been developed. The following classification is associated with the dependancy on the number of degrees of freedom (dofs) with respect to the number of layers:

- the Equivalent Single Layer approach (ESL): the number of unknowns is independent of the number of layers, but the transverse shear and normal stresses continuity on the interfaces between layers are often violated. The first work for one-layer isotropic plates was proposed in [1]. Then, we can distinguish the classical laminate theory [2] (it is based on the Euler–Bernoulli hypothesis and leads to inaccurate results for composites and moderately thick beams, because both transverse shear and normal strains are neglected), the first order shear deformation theory ([3], composite laminates [4]), and higher order theories [5–8]. Some of them take into account transverse normal deformation [9–11] with a higher order theory. All these studies are based on a displacement approach, although other approaches are formulated on the basis of mixed formulations [12,13].
- the layerwise approach (LW): the number of dofs depends on the number of layers. This theory aims at overcoming the restriction of the ESL concerning the discontinuity of out-of-plane stresses on the interface layers. This approach was introduced in [14,15], and also used in [16–18]. For recent contributions, see [19–22]. Again, some models which take into account the transverse normal effect have been developed: [23] within a displacement based approach and [24,25,12,26] within a mixed formulation.

In this framework, refined models have been developed in order to improve the accuracy of ESL models avoiding the additional computational cost of LW approach. Based on physical considerations and after some algebraic transformations, the number of unknowns becomes independent of the number of layers. Whitney [17] has extended the work of [27] for symmetric laminated composites with arbitrary orientation and a quadratic variation of the transverse stresses in each layer. So, a family of models, denoted zig-zag models, was derived (see [28–33]). Note also the refined approach based on the Sinus model [34–36]. This above literature deals with only some aspects of the broad research activity about models for layered structures and corresponding finite element formulations. An extensive assessment of different approaches has been made in [37–41].

Over the past years, the Proper Generalized Decomposition (PGD) has shown interesting features in the reduction model framework [42]. This type of method has been also introduced by Ladevèze [43] and called "radial approximation" in the Latin

* Corresponding author.
*E-mail address:* philippe.vidal@u-paris10.fr (P. Vidal).

method framework. It allows to decrease drastically computational time [44]. It has been also used in the context of separation of coordinate variables in multi-dimensional PDEs [42]. For a review about the PGD and its fields of applications, the reader can refer to [45,46].

In this work, a finite element based on the PGD for rectangular laminated beam analysis is built. The displacements are written under the form of separated variables representations, i.e. a sum of products of unidimensional polynomials of $x$ and $z$. The approximation of the 2D beam is based on a quadratic finite element (FE) approximation for the variation with respect to $x$ and a quadratic LW description for the variation with respect to $z$. Using the PGD, each unknown function of $x$ is classically approximated using one degree of freedom (dof) at the node of the mesh while the LW unknown functions of $z$ are global for the whole beam. Finally, the deduced non-linear problem implies the resolution of two linear problems alternatively. This process yields to few unknowns involved in each of these linear problems.

We now outline the remainder of this article. First the mechanical formulation is given. Then, the finite element discretization based on the Proper Generalized Decomposition is described. The principles of the approach are recalled in the framework of our study. It is illustrated by numerical tests which have been performed upon various isotropic, laminated and sandwich beams. A parametric study is given to show the effects of boundary conditions, length-to-thickness ratio and number of degrees of freedom. This set of numerical evaluations includes highly anisotropic structures. The accuracy of the results are evaluated by comparisons with an exact three-dimensional theory for laminates in bending [18] and also two-dimensional finite element computations using commercial finite element software.

## 2. Reference problem description

### 2.1. The governing equations

Let us consider a beam occupying the domain $\Omega = \Omega_x \times \Omega_z \times \left[-\frac{b}{2} \leqslant y \leqslant \frac{b}{2}\right] = [0, L] \times \left[-\frac{h}{2} \leqslant z \leqslant \frac{h}{2}\right] \times \left[-\frac{b}{2} \leqslant y \leqslant \frac{b}{2}\right]$ in a Cartesian coordinate $(x,y,z)$. The beam has a rectangular uniform cross section of height $h$, width $b$ and is assumed to be straight. The beam is made of $NC$ layers of different linearly elastic materials. Each layer may be assumed to be orthotropic in the beam axes. The $x$ axis is taken along the central line of the beam whereas $y$ and $z$ are the two axes of symmetry of the cross section intersecting at the centroid, see Fig. 1. As shown in this figure, the $y$ axis is along the width of the beam. This work is based upon a displacement approach for geometrically linear elastic beams.

In the following, the beam is considered in the $(x,z)$ plane, the $y$-coordinate is neglected.

#### 2.1.1. Constitutive relation

Each layer of the laminate is assumed to be orthotropic. Using matrix notation, the stress–strain law of the $k$th layer is given by:

$$\begin{bmatrix} \sigma_{11}^{(k)} \\ \sigma_{33}^{(k)} \\ \sigma_{13}^{(k)} \end{bmatrix} = \begin{bmatrix} \overline{C}_{11}^{(k)} & \overline{C}_{13}^{(k)} & 0 \\ & \overline{C}_{33}^{(k)} & 0 \\ symm & & \overline{C}_{55}^{(k)} \end{bmatrix} \begin{bmatrix} \varepsilon_{11}^{(k)} \\ \varepsilon_{33}^{(k)} \\ \varepsilon_{13}^{(k)} \end{bmatrix} \text{ i.e. } [\sigma^{(k)}] = [\overline{C}^{(k)}][\varepsilon^{(k)}] \qquad (1)$$

where we denote the stress $\sigma$ and the strain $\varepsilon$. $\overline{C}_{ij}^{(k)}$ are the moduli of the material for the $k$th layer taking into account the zero transverse normal stress hypothesis ($\sigma_{22} = 0$). They are expressed by

$$\overline{C}_{ij}^{(k)} = C_{ij}^{(k)} - C_{i2}^{(k)} C_{j2}^{(k)} / C_{22}^{(k)} \qquad (2)$$

where $C_{ij}^{(k)}$ are 3D stiffness coefficients. We also have $\overline{C}_{55}^{(k)} = C_{55}^{(k)}$.

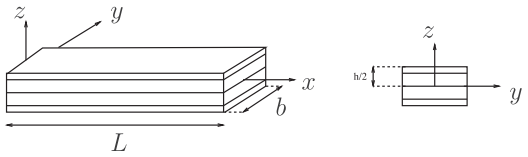


**Fig. 1.** The laminated beam and co-ordinate system.

#### 2.1.2. The weak form of the boundary value problem

Using the above matrix notation and for admissible displacement $\delta\vec{u} \in \delta U$, the Principle of Virtual Work is given by:

find $\vec{u} \in U$ (space of admissible displacements) such that

$$-\int_\Omega [\varepsilon(\delta\vec{u})]^T [\sigma(\vec{u})] d\Omega + \int_\Omega [\delta u]^T [b] d\Omega + \int_{\Gamma_F} [\delta u]^T [F] d\Gamma_F = 0 \quad \forall \delta\vec{u} \in \delta U \qquad (3)$$

where $[b]$ and $[F]$ are the prescribed body and surface forces applied on $\Gamma_F$.

### 2.2. The displacement field for the composite beam

In classical beam theory, the displacement field is assumed to be of the following form

$$u_1(x,z) = \sum_{i=0}^{N_1} z^i v_1^i(x) \qquad (4)$$

$$u_3(x,z) = \sum_{i=0}^{N_3} z^i v_3^i(x) \qquad (5)$$

where $(v_1^i, v_3^i)$ are the functions to be sought.

For instance, we can derive two models available in literature:

- the classical Timoshenko model with $N_1 = 1$ and $N_3 = 0$,
- ED2 model in Carrera's Unified Formulation [39] with $N_1 = 2$ and $N_3 = 2$.

## 3. Application of the Proper Generalized Method to beam

The Proper Generalized Decomposition (PGD) was introduced in [42] and is based on an *a priori* construction of separated variables representation of the solution. The following sections are dedicated to the introduction of PGD for beam analysis.

### 3.1. The displacement field

The displacement solution $(u_1(x,z), u_3(x,z))$ is constructed as the sum of $N$ products of functions of only one spatial coordinate ($N \in \mathbb{N}$ is the order of the representation)

$$\begin{aligned} u_1(x,z) &= \sum_{i=1}^{N} f_1^i(z) v_1^i(x) \\ u_3(x,z) &= \sum_{i=1}^{N} f_3^i(z) v_3^i(x) \end{aligned} \qquad (6)$$

where $(f_1^i, f_3^i)$ and $(v_1^i, v_3^i)$ are functions which must be computed during the resolution process. In this paper, polynomial expansions are used and only the coefficients of each polynomial expansion have to be computed. As an illustration the new unknowns are the $\left(a_{kj}^i\right)_{j=0,2}$ coefficients in

$f_k^i(z) = a_{k0}^i + a_{k1}^i z + a_{k2}^i z^2$ for $k \in \{1,3\}$

### 3.2. The problem to be solved

The relation (6) can be written in a more compact way

$$u = \sum_{i=1}^{N} F^i v^i = \sum_{i=1}^{N} V^i f^i \tag{7}$$

with the following notations

$$u = \begin{bmatrix} u_1(x,z) \\ u_3(x,z) \end{bmatrix}, \quad v^i = \begin{bmatrix} v_1^i(x) \\ v_3^i(x) \end{bmatrix}, \quad f^i = \begin{bmatrix} f_1^i(z) \\ f_3^i(z) \end{bmatrix}, \tag{8}$$

and

$$V^i = \begin{bmatrix} v_1^i(x) & 0 \\ 0 & v_3^i(x) \end{bmatrix} \text{ and } F^i = \begin{bmatrix} f_1^i(z) & 0 \\ 0 & f_3^i(z) \end{bmatrix} \tag{9}$$

Using this new separated representation, an iterative procedure must be introduced. If we assume that the first $n$ functions have been already computed, the solution for the iteration $n+1$ is written as

$$u = \bar{u} + Vf = \bar{u} + Fv \tag{10}$$

where $\bar{u}$ is the associated known set at iteration $n$ defined by

$$\bar{u} = \sum_{i=1}^{n} F^i v^i = \sum_{i=1}^{n} V^i f^i \tag{11}$$

and

$$v = \begin{bmatrix} v_1(x) \\ v_3(x) \end{bmatrix} \; f = \begin{bmatrix} f_1(z) \\ f_3(z) \end{bmatrix} \; V = \begin{bmatrix} v_1(x) & 0 \\ 0 & v_3(x) \end{bmatrix} \; F = \begin{bmatrix} f_1(z) & 0 \\ 0 & f_3(z) \end{bmatrix}$$

The new unknowns $(v,f)$ are computed such that (10) satisfies the weak Eq. (3). For sake of clarity the surfaces forces are neglected in the developments and the weak form of the beam problem introduced in Eq. (3) simplifies in

$$-\int_{\Omega_x}\int_{\Omega_z} ([\varepsilon(\delta u)]^T[C][\varepsilon(u)] + [\delta u]^T[b])dzdx = [0] \tag{12}$$

where $[C]$ represents, in each layer $(k)$, the matrix of the elastic moduli. Introducing $\delta u = V\delta f + F\delta v$ in Eq. (12), two equations are deduced

$$-\int_{\Omega_x}\int_{\Omega_z} ([\varepsilon(F\delta v)]^T[C][\varepsilon(\bar{u}+Fv)] + [F\delta v]^T[b])dzdx = [0] \tag{13}$$

$$-\int_{\Omega_x}\int_{\Omega_z} ([\varepsilon(V\delta f)]^T[C][\varepsilon(\bar{u}+Vf)] + [V\delta f]^T[b])dzdx = [0] \tag{14}$$

As these equations define a coupled non-linear problem, a non-linear resolution strategy has to be used. The simplest strategy is a fixed point method. An initial function $f^{(0)}$ is set, and at each step, the algorithm computes a new pair $(v^{(m+1)}, f^{(m+1)})$ such that

- $v^{(m+1)}$ satisfies Eq. (13) for $f$ set to $f^{(m)}$
- $f^{(m+1)}$ satisfies Eq. (14) for $v$ set to $v^{(m+1)}$

These two equations are linear and the first one has to be solved on $\Omega_x$, while the second one has to be solved on $\Omega_z$.

The fixed point algorithm is stopped when

$$\left[\int_{\Omega_x}\int_{\Omega_z} \left(v_1^{(m+1)}f_1^{(m+1)} - v_1^{(m)}f_1^{(m)}\right)^2 + \left(v_3^{(m+1)}f_3^{(m+1)} - v_3^{(m)}f_3^{(m)}\right)^2 dxdz\right]^{1/2} \leqslant \varepsilon \tag{15}$$

where $\varepsilon$ is a small enough parameter to be fixed by the user.

### 3.3. Variational problem defined on $\Omega_x$

For the sake of simplicity, the function $f^{(m)}$ which is assumed to be known, will be denoted $\bar{f}$ (and $\overline{F}$), and the function $v^{(m+1)}$ to be computed will be denoted $v$. The strain in Eq. (13) is defined in matrix notations as

$$[\varepsilon(\overline{F}v)] = [B_z(\bar{f})][\mathcal{E}_v] \tag{16}$$

with

$$[B_z(\bar{f})] = \begin{bmatrix} 0 & \bar{f}_1 & 0 & 0 \\ 0 & 0 & \bar{f}_3' & 0 \\ \bar{f}_1' & 0 & 0 & \bar{f}_3 \end{bmatrix} \text{ and } [\mathcal{E}_v] = \begin{bmatrix} v_1 \\ v_1' \\ v_3 \\ v_3' \end{bmatrix} \tag{17}$$

where the prime stands for the classical derivation (i.e. $v_1'(x) = \frac{dv_1}{dx}(x)$). The variational problem defined on $\Omega_x$ from Eq. (13) is

$$\int_{\Omega_x} [\delta\mathcal{E}_v]^T[k_z(\bar{f})][\mathcal{E}_v]dx = \int_{\Omega_x} [\delta v]^T[f_z(\bar{f})]dx - \int_{\Omega_x} [\delta\mathcal{E}_v]^T[\sigma_z(\bar{f},\bar{u})]dx \tag{18}$$

with

$$[k_z(\bar{f})] = \int_{\Omega_z} [B_z(\bar{f})]^T[C][B_z(\bar{f})]dz \tag{19}$$

$$[f_z(\bar{f})] = \int_{\Omega_z} \overline{F}^T[b]dz \tag{20}$$

$$[\sigma_z(\bar{f},\bar{u})] = \int_{\Omega_z} [B_z(\bar{f})]^T[C][\varepsilon(\bar{u})]dz \tag{21}$$

### 3.4. Variational problem defined on $\Omega_z$

In the following, the function $v^{(m+1)}$ which is assumed to be known, will be denoted $\bar{v}$ (and $\overline{V}$), and the function $f^{(m+1)}$ to be computed will be denoted $f$. The strain in Eq. (14) is defined in matrix notations as

$$[\varepsilon(\overline{V}f)] = [B_x(\bar{v})][\mathcal{E}_f] \tag{22}$$

with

$$[B_x(\bar{v})] = \begin{bmatrix} \bar{v}_1' & 0 & 0 & 0 \\ 0 & 0 & 0 & \bar{v}_3 \\ 0 & \bar{v}_1 & \bar{v}_3' & 0 \end{bmatrix} \text{ and } [\mathcal{E}_f] = \begin{bmatrix} f_1 \\ f_1' \\ f_3 \\ f_3' \end{bmatrix} \tag{23}$$

The variational problem defined on $\Omega_z$ from Eq. (14) is

$$\int_{\Omega_z} [\delta\mathcal{E}_f]^T[k_x(\bar{v})][\mathcal{E}_f]dz = \int_{\Omega_z} [\delta F]^T[f_x(\bar{v})]dz - \int_{\Omega_z} [\delta\mathcal{E}_f]^T[\sigma_x(\bar{v},\bar{u})]dz \tag{24}$$

with

$$[k_x(\bar{v})] = \int_{\Omega_x} [B_x(\bar{v})]^T[C][B_x(\bar{v})]dx \tag{25}$$

$$[f_x(\bar{v})] = \int_{\Omega_x} \overline{V}^T[b]dx \tag{26}$$

$$[\sigma_x(\bar{v},\bar{u})] = \int_{\Omega_x} [B_x(\bar{v})]^T[C][\varepsilon(\bar{u})]dx \tag{27}$$

## 4. Galerkin discretization

To build the beam finite element approximation, a discrete representation of the functions $(v,f)$ must be introduced. We use a classical finite element approximation in $\Omega_x$, and a polynomial expansion in $\Omega_z$. The elementary vector of degree of freedom (dof) associated with the finite element mesh in $\Omega_x$ is denoted $[q_e^v]$ and the vector of dof associated with the polynomial expansion in $\Omega_z$ is denoted $[q^f]$. The displacement fields and the strain

**Table 1**
Boundary conditions/loads.

| | BC | Load |
|---|---|---|
| C–F | Clamped/Free | Force at $x_1 = L$ |
| C–SP | Clamped/Free | Sinusoidal pressure |
| CC–SP | Clamped/Clamped | Sinusoidal pressure |
| SS–F | Simply-supported/Simply-supported | Force at $x_1 = L/2$ |
| SS–SP | Simply-supported/Simply-supported | Sinusoidal pressure |

fields (see Eqs. (16) and (22)) are determined from the values of $[q_e^v]$ and $[q^f]$ by

$$v_e = [N_x][q_e^v], \quad [\mathcal{E}_v^e] = [B_x][q_e^v], \quad f = [N_z][q^f] \text{ and } [\mathcal{E}_f] = [B_z][q^f] \tag{28}$$

The matrices $[N_x]$, $[B_x]$, $[N_z]$, $[B_z]$ contain the interpolation functions, their derivatives and the Jacobian components dependent on the chosen discrete representation. The fields $(\bar{v},\bar{f})$ built at each iteration of the fixed point method are defined by the vectors $[\bar{q}^v]$ and $[\bar{q}^f]$.

### 4.1. Approximation on $\Omega_x$

The introduction of (28) in the variational Eq. (18) leads to the linear system

$$[K_z(\bar{f})][q^v] = [\mathcal{R}_v(\bar{f},\bar{u})] \tag{29}$$

where $q^v$ is the vector of the nodal displacements associated with the finite element mesh in $\Omega_x$, $[K_z(\bar{f})]$ the stiffness matrix obtained by summing the elements' stiffness matrices $[K_z^e(\bar{f})]$ and $[\mathcal{R}_v(\bar{f},\bar{u})]$ the equilibrium residual obtained by summing the elements' residual load vectors $[\mathcal{R}_v^e(\bar{f},\bar{u})]$

$$[K_z^e(\bar{f})] = \int_{L_e} [B_x]^T [k_z(\bar{f})][B_x] dz \tag{30}$$

and

$$[\mathcal{R}_v^e(\bar{f},\bar{u})] = \int_{L_e} [N_x]^T [f_z(\bar{f})] dx - \int_{L_e} [B_x]^T [\sigma_z(\bar{f},\bar{u})] dx \tag{31}$$

### 4.2. Approximation on $\Omega_z$

The introduction of (28) in the variational Eq. (24) leads to the linear system

$$[K_x(\bar{v})][q^f] = [\mathcal{R}_f(\bar{v},\bar{u})] \tag{32}$$

where $[q^f]$ is the vector of degree of freedom associated with the polynomial expansion in $\Omega_z$, $[K_x(\bar{v})]$ is a stiffness matrix defined by (33) and $[\mathcal{R}_f(\bar{v},\bar{u})]$ an equilibrium residual defined by (34)

$$[K_x(\bar{v})] = \int_{\Omega_z} [B_z]^T [k_x(\bar{v})][B_z] dx \tag{33}$$

$$[\mathcal{R}_f(\bar{v},\bar{u})] = \int_{\Omega_z} [N_z]^T [f_x(\bar{v})] dz - \int_{\Omega_z} [B_z]^T [\sigma_x(\bar{v},\bar{u})] dz \tag{34}$$

**Table 3**
Convergence study with numerical layers – SS–SP – S = 4 – $N_x = 8$.

| $N_z$ | 1 | 2 | 4 | Reference |
|---|---|---|---|---|
| $Ndof_x + Ndof_z$ | 32 + 6 | 32 + 10 | 32 + 18 | |
| $\bar{w}(L/2,0)$ | 13.853 (1.8%) | 14.091 (0.1%) | 14.1084 (0.01%) | 14.107 |
| $\bar{\sigma}_{11}(L/2,h/2)$ | 9.7870 (1.7%) | 10.0100 (0.5%) | 10.0020 (0.4%) | 9.9556 |
| $\bar{\sigma}_{13}(0,0)$ | 1.3678 (28%) | 2.1763 (14%) | 1.9672 (3%) | 1.9012 |

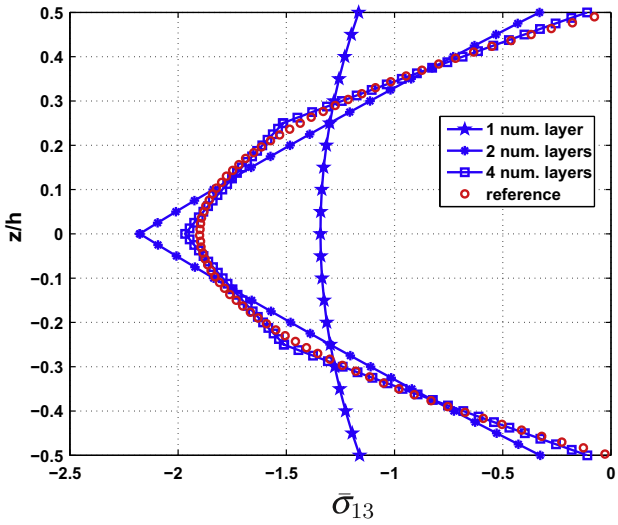


**Fig. 2.** Distribution of $\sigma_{13}$ along the thickness – numerical layers-isotropic-SS–SP–$S = 4 - N_x = 8$.

## 5. Numerical results

In this section, several static tests are presented validating our approach and evaluating its efficiency. A classical quadratic finite element is used for the unknowns depending on the $x$-axis coordinate. For the transverse direction, a quadratic layer-wise description is chosen. The present model is herein denoted by the acronym B2LD2-PGD as a reference to the nomenclature from [39]. B2 refers to the quadratic beam FE, LD2 means a layer-wise approach in a displacement formulation with a second order expansion in $z$. The properties of our method are assessed: convergence study and effect of the aspect ratio. Then, the influence of the boundary conditions is addressed. Finally, the flexural behaviour of highly inhomogeneous laminated and sandwich beams is analysed.

For all these tests, the different boundary conditions and their associated acronym are summarized in Table 1. The numbers of dofs are also precised for the two problems associated to $(v_1^i, v_3^i)$ and $(f_1^i, f_3^i)$. They are denoted $Ndof_x$ and $Ndof_z$ respectively.

Notice also that the convergence velocity of the fixed point process (cf. Section 3.2) is high. Usually, only a maximum of three iterations is required to reach the convergence as in [45].

**Table 2**
Convergence study – SS–SP – isotropic – S = 4.

| $N_x$ | 1 | 2 | 4 | 8 | 16 | 32 | 64 |
|---|---|---|---|---|---|---|---|
| $Ndof_x + Ndof_z$ | 4 + 6 | 8 + 6 | 16 + 6 | 32 + 6 | 64 + 6 | 128 + 6 | 256 + 6 |
| $\bar{w}(L/2,0)$ | 13.1438 | 13.8011 | 13.8497 | 13.8528 | 13.8531 | 13.8531 | 13.8531 |
| $\bar{\sigma}_{11}(L/2,h/2)$ | 10.035 | 10.140 | 9.8778 | 9.7870 | 9.7626 | 9.7564 | 9.7548 |
| $\bar{\sigma}_{13}(0,0)$ | 2.4950 | 1.8026 | 1.4658 | 1.3678 | 1.3423 | 1.3359 | 1.3343 |
| $\bar{\sigma}_{33}(L/2,h/2)$ | 1.2514 | 1.1447 | 1.0553 | 1.0273 | 1.0199 | 1.0181 | 1.0176 |

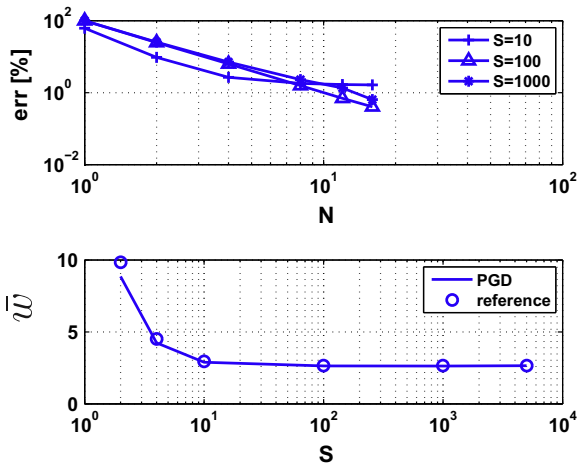


**Fig. 3.** Locking study – clamped/clamped – sinusoidal pressure – isotropic – $N_x = 8$ (bottom) – $N_z = 1$.

**Table 4**
Number of couples with respect to the boundary conditions/loads – $N_x = 16$.

| S | 4 | 10 | 100 |
|---|---|---|---|
| C–F | 4 | 4 | 3 |
| C–SP | 3 | 3 | 3 |
| SS–F | 2 | 2 | 1 |
| SS–SP | 1 | 1 | 1 |

In the following, the beam is discretized with $N_x$ elements. For the transverse approximation, a physical layer is discretized by one numerical layer. The use of more numerical layers is also evaluated. The number of numerical layer is denoted $N_z$. This strategy allows to improve the accuracy of the results as in [47] and [48].

As far as the computational cost is concerned, the present process requires two or three resolutions of two linear problems including $Ndof_x$ and $Ndof_z = 4 \times N_z + 2$ dofs respectively. In a classical layerwise FE approach, the calculation implies one linear resolution with $Ndof_x \times Ndof_z$ dofs. The computational gain becomes important when the number of numerical layers and the number of elements increase.

### 5.1. Properties of the approach

In this section, the properties of the PGD approach are assessed:

- a convergence study
  The influences of the refinement of the mesh with respect to the length and the number of numerical layers in the thickness are addressed.
- the length-to-thickness ratio

A simply-supported and clamped–clamped isotropic beam is considered with the following characteristics:

**geometry:** isotropic beam with length-to-thickness ratio $S = L/h$
**boundary conditions:** the beam is subjected to a sinusoidal pressure which is expressed as $q(x) = q_0 \sin\left(\frac{\pi x}{L}\right)$.
**material properties:** $E = 10^6$ MPa, $\nu = 0.3$
**mesh:** half of the beam is meshed. $N_x$ varies from 1 to 64.
**results:** the results $(\bar{w}, \bar{\sigma}_{11}, \bar{\sigma}_{13}, \bar{\sigma}_{33})$ are made non-dimensional using:

$$\bar{w} = u_3(L/2, 0)\frac{100Eh^3}{q_0 L^4}, \quad \bar{\sigma}_{ij} = \sigma_{ij}\frac{1}{q_0} \text{ for } \begin{cases} \sigma_{11}, \sigma_{33}(L/2, h/2) \\ \sigma_{13}(0, 0) \end{cases}$$

The reference solution is issued from a 2D elasticity analysis with a very refined mesh including 3800 dofs in ANSYS. The element PLANE82 is used.

#### 5.1.1. Convergence study

Table 2 gives the convergence of the present model for the transverse displacement, the in-plane, transverse shear and transverse normal stresses for $S = 4$. One numerical layer through the thickness is used. The number of dofs of each linear problem is also precised. The convergence velocity is very high. Based on progressive mesh refinement, a $N_x = 8$ mesh is adequate to model the thick isotropic beam for a bending analysis. The difference compared with results issued from a $N_x = 64$ mesh becomes less than 2.5%. Note that the deflection is insensitive to the mesh.

Based on this result, the influence of the numerical layer is given in Table 3 using the $N_x = 8$ mesh. A physical layer can be divided into several numerical layers. The error rate decreases when the number of numerical layers increases for the displacement and the stresses. The transverse shear stress is very sensitive to this refinement. Fig. 2 shows the distribution through the thickness of $\sigma_{13}$. As it is expected, the quadratic approximation is not a good choice for recovering a parabolic distribution. Therefore, more numerical layers are needed.

#### 5.1.2. Shear locking phenomenon

Considering various values for the aspect ratio, the normalized displacement obtained at the middle of the clamped–clamped isotropic beam is shown in Fig. 3 (bottom) along with a reference solution, and they are found to be in excellent agreement. From Fig. 3 (top), we notice that the velocity convergence is independent of the slenderness ratio. So, it is inferred from Fig. 3 that the present element is free from the shear locking phenomenon.

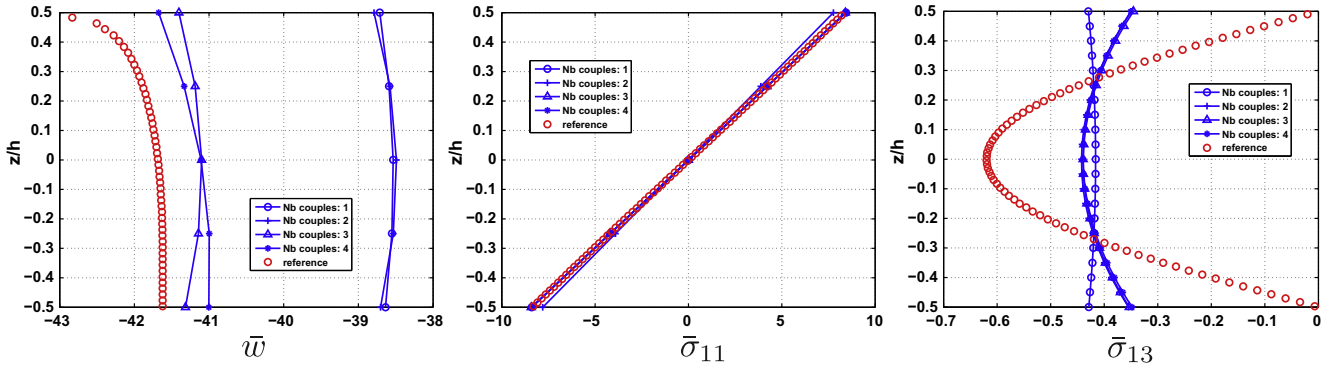


**Fig. 4.** Distribution of $\bar{w}$ (left), $\bar{\sigma}_{11}$ (middle) and $\bar{\sigma}_{13}$ (right) along the thickness – $S = 4$ – isotropic – CF.

**Table 5**
Three layers (0°/90°/0°) – SS–SP – $N_x = 8$ – sr (6) – $N_z = NC$.

| S | Model | $\bar{u}(0, h/2)$ | $\bar{w}(L, 0)$ | $\bar{\sigma}_{11}(L/2, h/2)$ | $\bar{\sigma}_{13}(0, 0)$ |
|---|---|---|---|---|---|
| 4 | Exact | −0.9456 | 2.8899 | 18.820 | 1.432 |
| | B2LD2-PGD | −0.9304 (1.6%) | 2.8664 (0.8%) | 18.536 (1.5%) | 1.417 (1.0%) |
| 20 | Exact | −66.9407 | 0.6185 | 263.163 | 8.7483 |
| | B2LD2-PGD | −66.9380 (0.0%) | 0.6184 (0.0%) | 263.220 (0.0%) | 8.7451 (0.0%) |
| 40 | Exact | −519.115 | 0.5379 | 1019.68 | 17.641 |
| | B2LD2-PGD | −519.160 (0.0%) | 0.5377 (0.0%) | 1020.00 (0.0%) | 17.690 (0.3%) |
| 100 | Exact | −8038.46 | 0.5152 | 6314.56 | 44.206 |
| | B2LD2-PGD | −8039.60 (0.0%) | 0.5140 (0.2%) | 6316.70 (0.0%) | 45.274 (2.4%) |

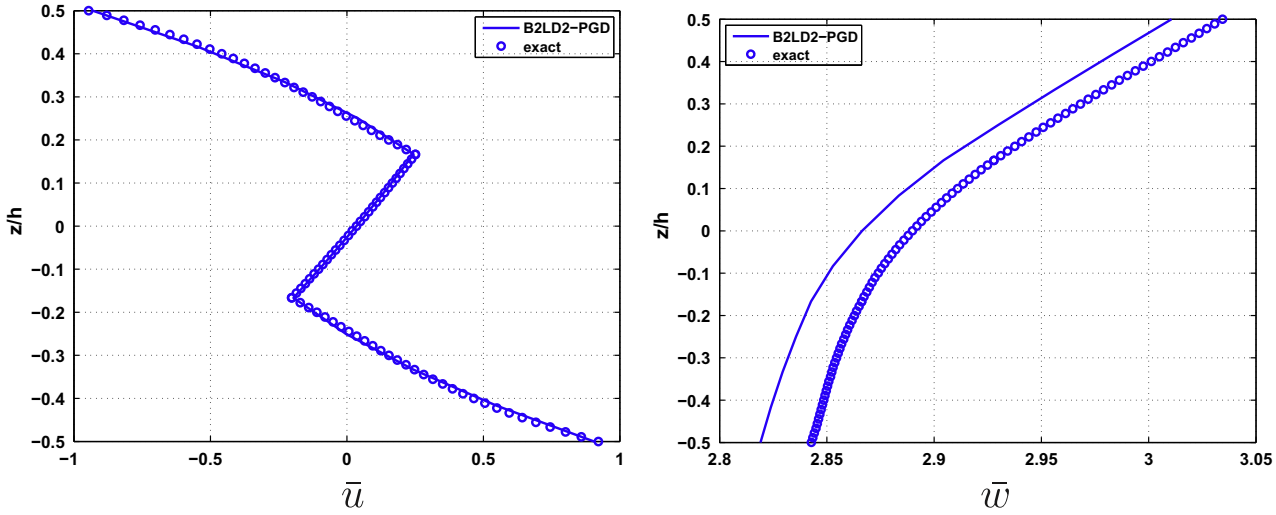


**Fig. 5.** Distribution of $\bar{u}$ (left) and $\bar{w}$ (right) along the thickness – $S = 4$–3 layers (0°/90°/0°) – $N_z = NC$.

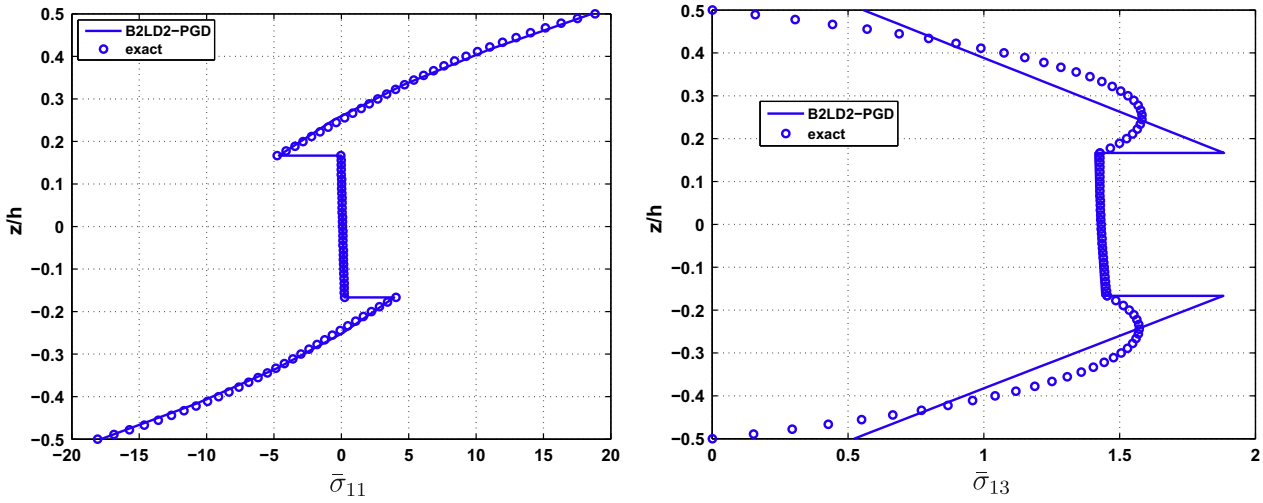


**Fig. 6.** Distribution of $\bar{\sigma}_{11}$ (left) and $\bar{\sigma}_{13}$ (right) along the thickness – $S = 4$–3 layers (0°/90°/0°) – $N_z = NC$.

### *5.2. Influence of the boundary conditions*

The influence of the boundary conditions and the type of loads on the number of couples $(f_1^i(z), v_1^i(x))$, $(f_3^i(z), v_3^i(x))$ (Cf. Eq. (6)) is summarized in Table 4. The configuration and the notation are given in Section 5. As expected, the C–F case needs more couples than the other cases, and the number of terms is also sensitive to the aspect ratio.

For the more severe case, Fig. 4 shows the distribution of $(\bar{w},\ \bar{\sigma}_{11},\ \bar{\sigma}_{13})$ with respect to the number of couples. During this iterative process, the transverse displacement is strongly improved, while the stresses are not too much modified. It is

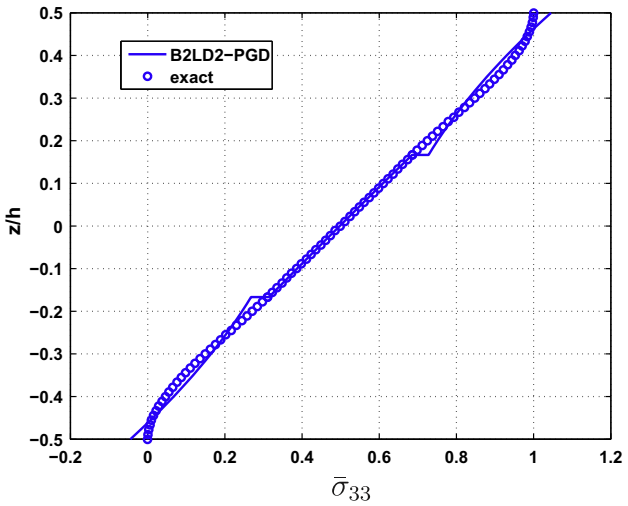


**Fig. 7.** Distribution of $\bar{\sigma}_{33}$ along the thickness – S = 4–3 layers (0°/90°/0°) – $N_z$ = *NC*.

necessary to have additional numerical layers to recover the parabolic distribution of $\sigma_{13}$ as in Section 5.1 (Cf. Fig. 2).

### 5.3. Bending analysis of laminated composite beam

To see the capability of the present approach to model laminated composite beam, symmetric and antisymmetric beams are considered as in [18]. It is detailed below:

**geometry:** composite cross-ply beam (0°/90°/0°), (0°/90°/0°/90°) and length-to-thickness ratio $S = 4/20/40/100$. All layers have the same thickness.
**boundary conditions:** simply supported beam subjected to sinusoidal load $q(x) = q_0 \sin\frac{\pi x}{L}$.
**material properties:**

$$E_L = 172.4 \text{ GPa}, E_T = 6.895 \text{ GPa}, G_{LT} = 3.448 \text{ GPa},$$
$$G_{TT} = 1.379 \text{ GPa}, \ \nu_{LT} = \nu_{TT} = 0.25$$

where $L$ refers to the fiber direction, $T$ refers to the transverse direction.

**mesh:** half of the beam is meshed. $N_x = 8$ with spacing ratio (6) (denoted sr (6)), $\frac{L_{emax}}{L_{emin}} = 6$, where $L_{e\ \max}$ and $L_{e\ \min}$ are the maximal and minimal length of the elements. The mesh is refined near the two edges of the finite element model.

**number of dofs:** $Ndof_x = 32$ and $Ndof_z = 4 \times N_z + 2$
**results:** The results $(\bar{u}, \bar{w}, \bar{\sigma}_{11}, \bar{\sigma}_{13})$ are made non-dimensional using:

$$\bar{u} = u_1(0, h/2)\frac{E_T}{hq_0} \quad \bar{w} = u_3(L/2, 0)\frac{100E_T}{S^4 hq_0}$$
$$\bar{\sigma}_{ij} = \sigma_{ij}\frac{1}{q_0} \text{ for } \begin{cases} \sigma_{11}(L/2, h/2) \\ \sigma_{13}(0, 0) \end{cases} \tag{35}$$

The three layers case (0°/90°/0°) is first presented. The numerical results for deflection, in-plane displacement, shear stress, and in-plane stress are given in Table 5 with respect to span-to-thickness ratio: $S = 4$ (thick), $S = 20$ (moderately thick), $S = 40$ (thin), $S = 100$ (very thin). The percent error with respect to the exact solution [18] is also given in this table. We observe that the present approach performs very well with respect to this exact solution. The maximum error rate is less than 2.4% whatever the slenderness ratio.

For the ratio $S = 4$ (the most critical test), the normalized in-plane, transverse shear, normal stresses, and the transverse displacement are presented in Figs. 5–7. These distributions are in excellent agreement with the reference solutions, excepted for $\sigma_{13}$ in Fig. 6 right. The variation of the transverse shear stress is linear in each layer, due to the choice of the quadratic LW description for the functions $f_k^i(z)$. Moreover, the continuity of the transverse shear stress at the interface is not fulfilled. To improve this result, it is necessary to divide each layer into a minimum of 2 numerical layers. The corresponding distributions of $\bar{\sigma}_{13}$ and $\bar{\sigma}_{33}$ through the thickness are given in Fig. 8. The improvement is evident.

Note that the model can be viewed as a zig-zag one (see Fig. 5 left).

Next we consider the four-layer case (0°/90°/0°/90°). The results are summarized in Table 6. Figs. 9–11 show the in-plane and out-of-plane displacements, the in-plane, transverse normal and shear stresses for the more severe case ($S = 4$). All results are satisfactory with respect to the exact solution for $S = 4$, 20, 40, 100. The maximum error rate is 0.4% for the displacements and 4% for the stresses. The use of more numerical layers improves the accuracy of the results for both transverse shear and normal stresses (see Fig. 12).

### 5.4. Bending analysis of sandwich beam

This test deals with a sandwich beam under a sinusoidal pressure with a high value of face-to-core stiffness ratio. This severe

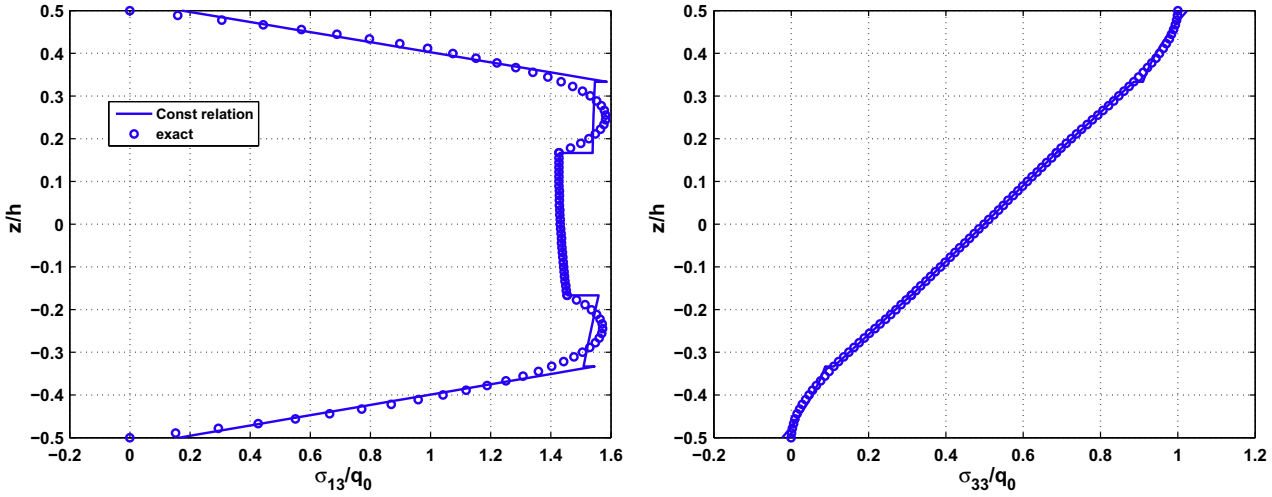


**Fig. 8.** Distribution of $\bar{\sigma}_{13}$ (left) and $\bar{\sigma}_{33}$ (right) along the thickness – S = 4–3 layers – $N_z = 2 \times NC$.

**Table 6**
Four layers (0°/90°/0°/90°) – SS–SP – $N_x = 8$ sr (6) – $N_z = NC$.

| S | Model | $\bar{u}(0, h/2)$ | $\bar{w}(L, 0)$ | $\bar{\sigma}_{11}(L/2, h/2)$ | $\bar{\sigma}_{13}(0, 0)$ |
|---|---|---|---|---|---|
| 4 | Exact | −3.0275 | 4.1846 | 2.6278 | 1.9224 |
| | B2LD2-PGD | −3.0143 (0.4%) | 4.1702 (0.3%) | 2.6218 (0.2%) | 1.9125 (0.5%) |
| 20 | E | −184.217 | 1.2627 | 29.1867 | 11.2757 |
| | B2LD2-PGD | −184.224 (0.0%) | 1.2624 (0.0%) | 29.2010 (0.0%) | 11.3290 (0.5%) |
| 40 | Exact | −1415.01 | 1.1616 | 111.3850 | 22.6850 |
| | B2LD2-PGD | −1415.16 (0.0%) | 1.1605 (0.1%) | 111.4500 (0.1%) | 22.9170 (1.0%) |
| 100 | Exact | −21850.43 | 1.1331 | 686.7017 | 56.8072 |
| | B2LD2-PGD | −21853.00 (0.0%) | 1.1291 (0.4%) | 687.1800 (0.1%) | 59.4660 (4%) |

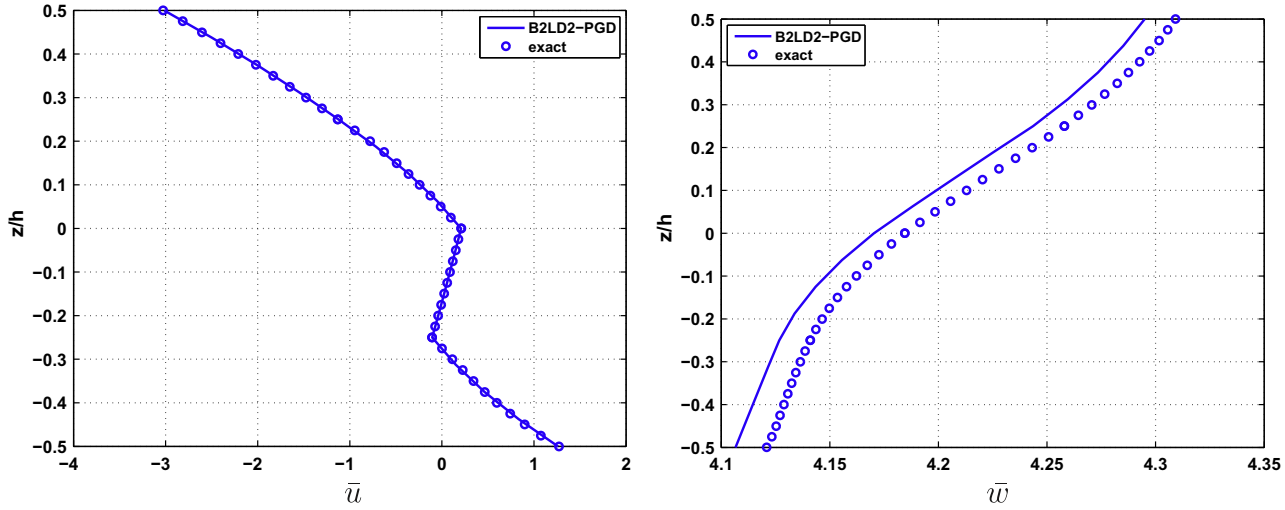


**Fig. 9.** Distribution of $\bar{u}$ (left) and $\bar{w}$ (right) along the thickness – S = 4–4 layers (0°/90°/ 0°/90°) – $N_z = NC$.

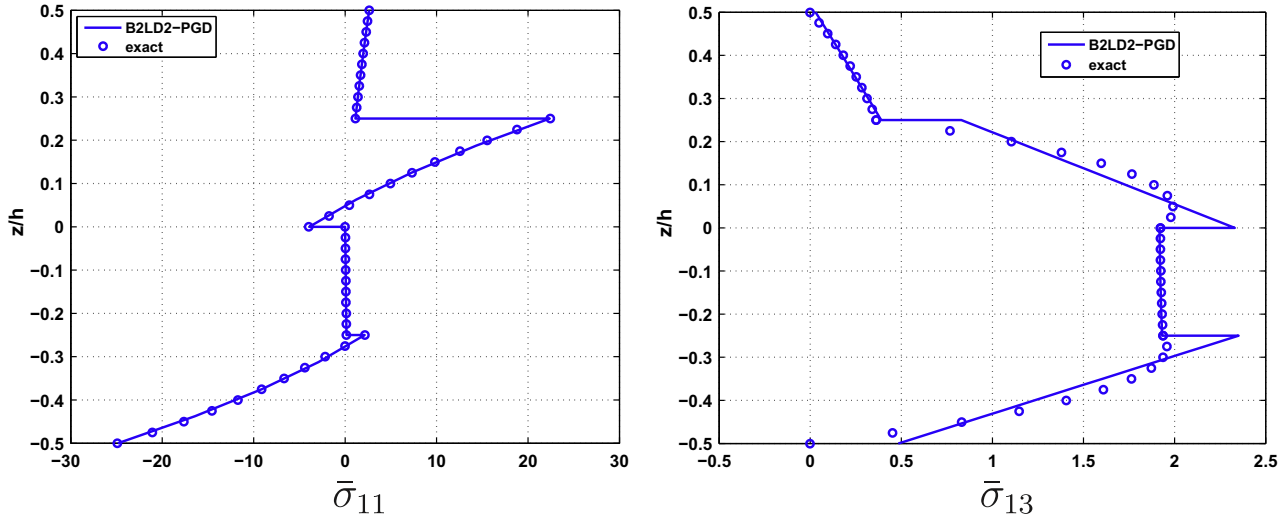


**Fig. 10.** Distribution of $\bar{\sigma}_{11}$ (left) and $\bar{\sigma}_{13}$ (right) along the thickness – S = 4–4 layers (0°/90°/0°/90°) – $N_z = NC$.

test allows us to evaluate the capability of the model for a high anisotropic beam. This case has already been studied in [49].

This example is detailed now.

**geometry:** the 3-layer sandwich beam has aluminium alloy faces and a soft core with thickness 0.1 h/0.8 h/0.1 h and length-to-thickness ratio $S = 4$.

**boundary conditions:** simply supported (SS–SP) beam under a sinusoidal pressure $q(x) = q_0 \sin\left(\frac{\pi x}{L}\right)$
**material properties:** face: $E_f = 73{,}000$ MPa, $\nu = 0.34$. Core: $E_c = \eta E_f$, with $\eta = 10^{-5}$
**mesh:** $N_x = 16$ sr (8), half of the beam is meshed.
**number of dofs:** $Ndof_x = 64$ and $Ndof_z = 4 \times NC + 2$
**results:** the results $(\bar{u}, \bar{w}, \bar{\sigma}_{11}, \bar{\sigma}_{13})$ are made non-dimensional using:

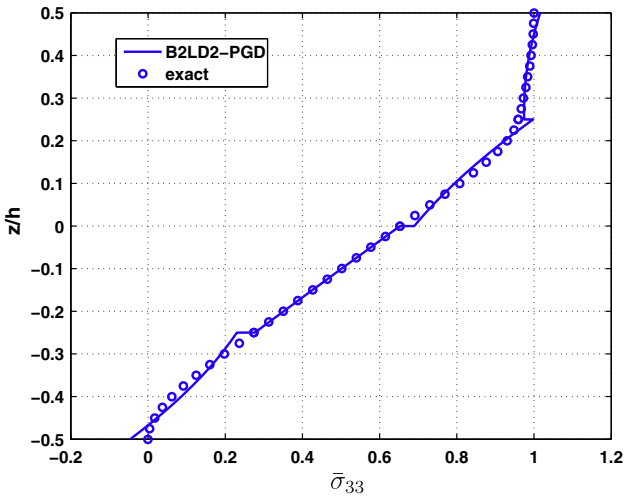


**Fig. 11.** Distribution of $\bar{\sigma}_{33}$ along the thickness – S = 4–4 layers (0°/90°/0°/90°) – $N_z = NC$.

$$\bar{u} = u_1(0,-h/2)\frac{E_f}{hq_0} \quad \bar{w} = u_3(L/2,0)\frac{100E_f}{S^4hq_0}$$
$$\bar{\sigma}_{ij} = \sigma_{ij}\ \frac{1}{q_0}\ \text{for}\ \begin{cases}\sigma_{11}(L/2,-h/2)\\ \sigma_{13}(0,0)\end{cases} \tag{36}$$

They are compared with results from a commercial code with a very refined mesh including 3800 dofs.

The distributions of $\bar{u}$, $\bar{w}$, $\bar{\sigma}_{11}$, $\bar{\sigma}_{13}$ and $\bar{\sigma}_{33}$ through the thickness are shown in Figs. 13–15. We notice that all these quantities have a complex behavior. The distribution of the in-plane displacement through the thickness is not linear and a strong discontinuity of the slope occurs at the interface between the bottom face and the core. The distributions of the stresses are non-symmetric, and rather different in the top and bottom faces. Finally, for this severe case, the results issued from the present approach are in very good agreement with the reference solution.

## 6. Conclusion and future prospects

In this article, a beam finite element based on the PGD has been presented and evaluated through different benchmarks. The PGD

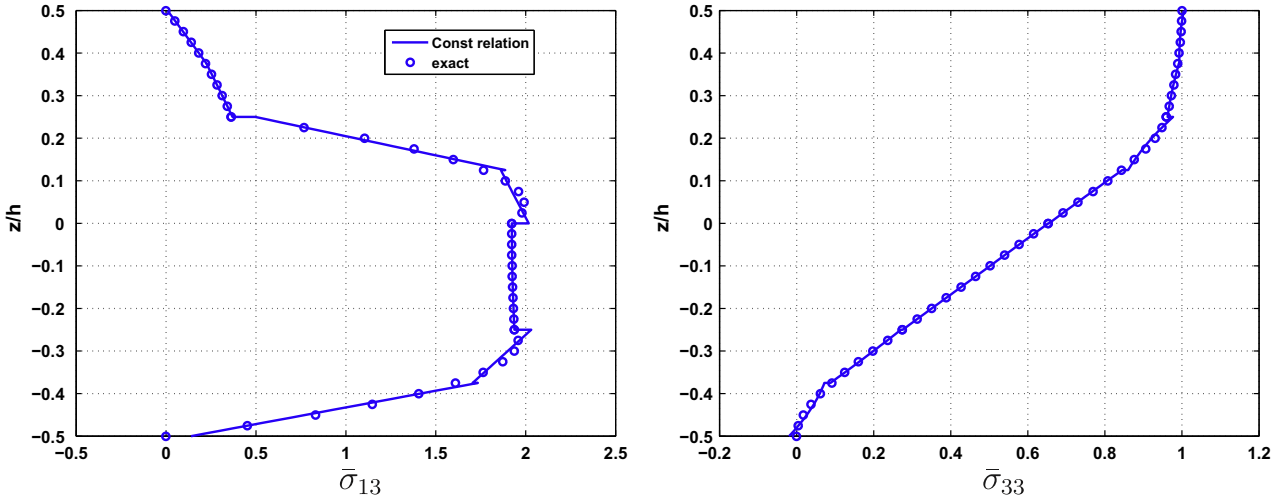


**Fig. 12.** Distribution of $\bar{\sigma}_{13}$ (left) and $\bar{\sigma}_{33}$ (right) along the thickness – S = 4–4 layers (0°/90°/0°/90°) – $N_z = 2 \times NC$.

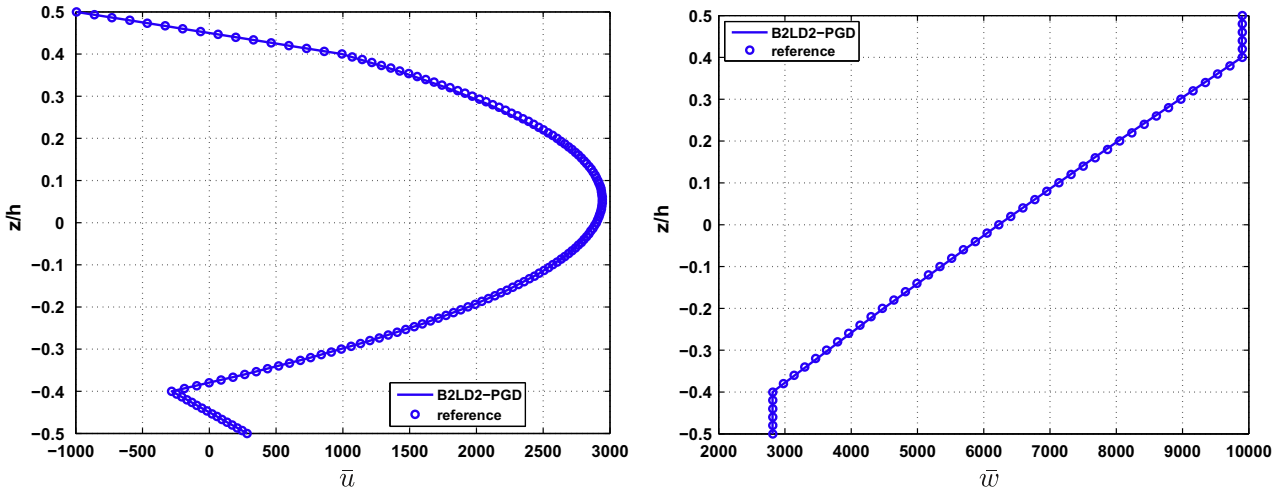


**Fig. 13.** Distribution of $\bar{u}$ (left) and $\bar{w}$ (right) along the thickness – S = 4 – sandwich – $N_z = NC$.

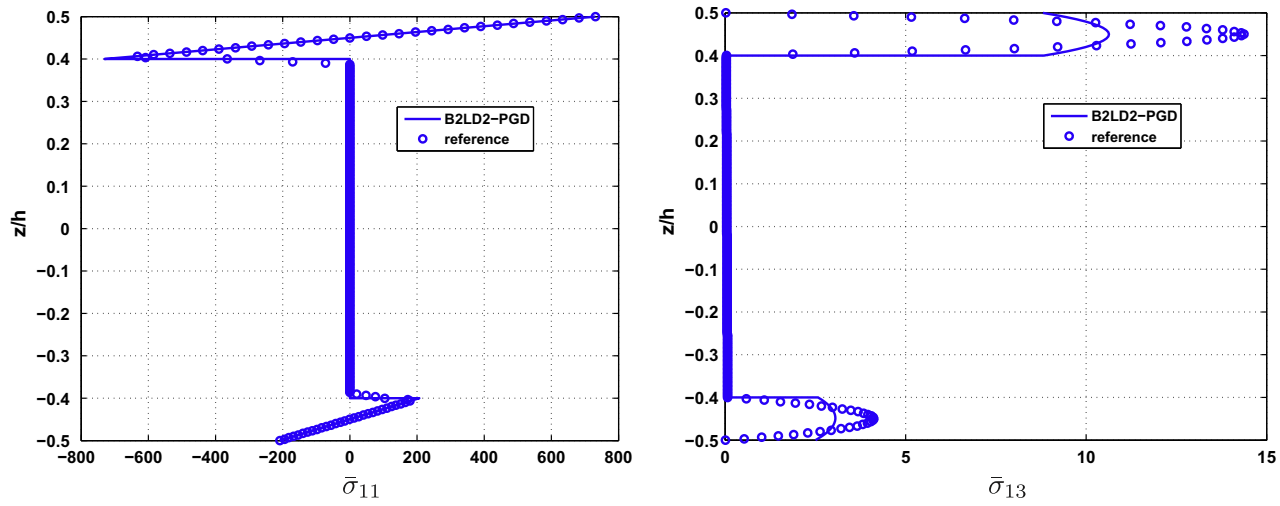


**Fig. 14.** Distribution of $\bar{\sigma}_{11}$ (left) and $\bar{\sigma}_{13}$ (right) along the thickness – S = 4 – sandwich – $N_z = NC$.

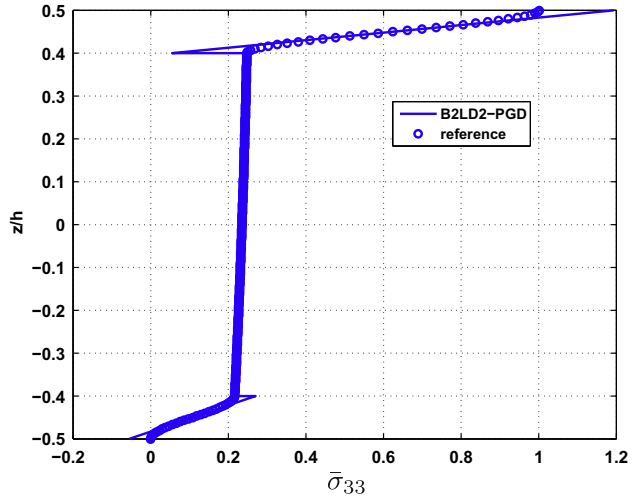


**Fig. 15.** Distribution of $\bar{\sigma}_{33}$ along the thickness – S = 4 – sandwich – $N_z = NC$.

approach allows to express the displacement as a separated representation of two 1D space functions. For the axial coordinate, classical 3-node FE is used while a quadratic layerwise description is introduced for the transverse coordinate. The derived iterative process implies the resolution of two 1D problems and the total cost depends on the number of couples representing the solution. This method has been applied to the modeling of laminated and sandwich composite. Several numerical evaluations have proved that it has very good properties. The convergence rate is high and accurate results are obtained for very thick to thin beams. The influence of the boundary conditions has been also addressed. This FE based on the PGD is accurate and less costly than layerwise FE or plane elasticity model in commercial software. Moreover, numerical layers can be introduced to improve the accuracy of the results with few additional computational times.

Based on these promising results, the use of the PGD for layerwise plate FE will be carried out. Furthermore, the PGD can be used to define the utmost terms of the expansion in the thickness, regarding the boundary conditions, the geometry and the material properties.

## References


[1] Basset AB. On the extension and flexure of cylindrical and spherical thin elastic shells. Philos Trans Royal Soc (London) Ser A 1890;181:433–80.
[2] Tanigawa Y, Murakami H, Ootao Y. Transient thermal stress analysis of a laminated composite beam. J Therm Stresses 1989;12:25–39.
[3] Mindlin RD. Influence of rotatory inertia and shear on flexural motions of isotropic, elastic plates. J Appl Mech ASME 1951;18:31–8.
[4] Yang PC, Norris CH, Stavsky Y. Elastic wave propagation in heterogeneous plates. Int J Solids Struct 1966;2:665–84.
[5] Librescu L. On the theory of anisotropic elastic shells and plates. Int J Solids Struct 1967;3:53–68.
[6] Whitney JM, Sun CT. A higher order theory for extensional motion of laminated composites. J Sound Vib 1973;30:85–97.
[7] Lo KH, Christensen RM, Wu FM. A higher-order theory of plate deformation. Part II: Laminated plates. J Appl Mech ASME 1977;44:669–76.
[8] Reddy JN. A simple higher-order theory for laminated composite plates. J Appl Mech ASME 1984;51(4):745–52.
[9] Matsunaga H. Assessment of a global higher-order deformation theory for laminated composite and sandwich plates. Compos Struct 2002;56:279–91.
[10] Kant T, Swaminathan K. Analytical solutions for the static analysis of laminated composite and sandwich plates based on a higher order refined theory. Compos Struct 2002;56:329–44.
[11] Cook GM, Tessler A. A {3,2}-order bending theory for laminated composite and sandwich beams. Compos Part B: Eng J 1998;29B:565–76.
[12] Carrera E. A priori vs. a posteriori evaluation of transverse stresses in multilayered orthotropic plates. Compos Struct 2000;48(4):245–60.
[13] Kim J-S, Cho M. Enhanced first-order theory based on mixed formulation and transverse normal effect. Int J Solids Struct 2007;44:1256–76.
[14] Heller RA, Swift GW. Solutions for the multilayer timoshenko beam. In Report N VPI-E-71-12. Virginia Polytechnic Institute, Blacksburg, VA, 1971.
[15] Swift GW, Heller RA. Layered beam analysis. J Eng Mech ASCE 1974;100:267–82.
[16] Srinivas S. A refined analysis of laminated composites. J Sound Vib 1973:495–507.
[17] Whitney JM. The effect of transverse shear deformation in the bending of laminated plates. J Comp Mater 1969;3:534–47.
[18] Pagano NJ. Exact solutions for composite laminates in cylindrical bending. J Comp Mater 1969;3:398–411.
[19] Shimpi RP, Ainapure AV. A beam finite element based on layerwise trigonometric shear deformation theory. Compos Struct 2001;53:153–62.
[20] Reddy JN. On refined computational models of composite laminates. Int J Numer Methods Eng 1989;27:361–82.
[21] Ferreira AJM. Analysis of composite plates using a layerwise shear deformation theory and multiquadrics discretization. Mech Adv Mater Struct 2005;12:99–112.
[22] Karger L, Wetzel A, Rolfes R, Rohwer K. A three-layered sandwich element with improved transverse shear stiffness and stresses based on FSDT. Comput Struct 2006;84:843–54.
[23] Icardi U. Higher-order zig-zag model for analysis of thick composite beams with inclusion of transverse normal stress and sublaminates approximations. Compos Part B: Eng J 2001;32:343–54.
[24] Rao MK, Desai YM. Analytical solutions for vibrations of laminated and sandwich plates using mixed theory. Compos Struct 2004;63:361–73.
[25] Carrera E. A study of transverse normal stress effect on vibration of multilayered plates and shells. J Sound Vib 1999;225:803–29.

[26] Carrera E. On the use of the Murakami's zig-zag function in the modeling of layered plates and shells. Comput Struct 2004;82:541–54.
[27] Ambartsumyan SA. Theory of anisotropic plates. Translated from Russian by T. Cheron and Edited by J.E. Ashton, Technomic Publishing Co., 1969.
[28] Di Sciuva M. Bending, vibration and buckling of simply supported thick multilayered orthotropic plates: an evaluation of a new displacement model. J Sound Vib 1986;105:425–42.
[29] Bhaskar K, Varadan TK. Refinement of higher-order laminated plate theories. AIAA J 1989;27:1830–1.
[30] Lee C-Y, Liu D, Lu X. Static and vibration analysis of laminated composite beams with an interlaminar shear stress continuity theory. Int J Numer Method Eng 1992;33:409–24.
[31] Cho M, Parmerter R. Efficient higher-order composite plate theory for general lamination configurations. AIAA J 1993;31:1299–306.
[32] Di Sciuva M, Icardi U. Numerical assessment of the core deformability effect on the behavior of sandwich beams. Compos Struct 2001;52:41–53.
[33] Kapuria S, Dumir PC, Ahmed A. An efficient higher order zigzag theory for composite and sandwich beams subjected to thermal loading. Int J Solids Struct 2003;40:6613–31.
[34] Vidal P, Polit O. A family of sinus finite elements for the analysis of rectangular laminated beams. Compos Struct 2008;84:56–72. http://dx.doi.org/10.1016/j.compstruct.2007.06.009.
[35] Vidal P, Polit O. A refined sine-based finite element with transverse normal deformation for the analysis of laminated beams under thermomechanical loads. J Mech Mater Struct 2009;4(6):1127–55.
[36] Vidal P, Polit O. A sine finite element using a zig-zag function for the analysis of laminated composite beams. Compos Part B: Eng J 2011;42(6):1671–82. http://dx.doi.org/10.1016/j.compositesb.2011.03.012.
[37] Noor AK, Burton WS. Assessment of computational models for multilayered composite shells. Appl Mech Rev 1990;43(4):67–97.
[38] Reddy JN. Mechanics of laminated composite plates – theory and analysis. Boca Raton, FL: CRC Press; 1997.
[39] Carrera E. Theories and finite elements for multilayered, anisotropic, composite plates and shells. Arch Comput Method Eng 2002;9:87–140.
[40] Carrera E. Historical review of zig-zag theories for multilayered plates and shells. Appl Mech Rev 2003;56(3):287–308.
[41] Zhang YX, Yang CH. Recent developments in finite elements analysis for laminated composite plates. Compos Struct 2009;88:147–57.
[42] Ammar A, Mokdada B, Chinesta F, Keunings R. A new family of solvers for some classes of multidimensional partial differential equations encountered in kinetic theory modeling of complex fluids. J Non-Newtonian Fluid Mech 2011;139:153–76.
[43] Ladevèze P. Nonlinear computational structural mechanics – new approaches and non-incremental methods of calculation. Springer-Verlag; 1999.
[44] Allix O, Vidal P. A new multi-solution approach suitable for structural identification problems. Comput Methods Appl Mech Eng 2002;191(25–26):2727–58.
[45] Nouy A. A priori model reduction through proper generalized decomposition for solving time-dependent partial differential equations. Comput Methods Appl Mech Eng 2010;199(23–24):1603–26.
[46] Chinesta F, Ammar A, Leygue A, Keunings R. An overview of the proper generalized decomposition with applications in computational rheology. J Non-Newtonian Fluid Mech 2011;166(11):578–92.
[47] Flanagan G. A general sublaminate analysis method for determining strain energy release rates in composites. CP AIAA 1994;94(1356):381–9.
[48] Averill RC, Yip YC. Thick beam theory and finite element model with zig-zag sublaminate approximations. AIAA J 1996;34(8):1627–32.
[49] Brischetto S, Carrera E, Demasi L. Improved bending analysis of sandwich plates using zig-zag function. Compos Struct 2009;89:408–15.